

Detection of Spaceborne Lasers with the Pierre Auger Observatory

Michael Unger^{a,*} for the Pierre Auger Collaboration^b and Oliver Lux^c and Oliver Reitebuch^c

^a*Institute for Astroparticle Physics, Karlsruhe Institute of Technology (KIT), 76131 Karlsruhe, Germany*

^b*Observatorio Pierre Auger, Av. San Martín Norte 304, 5613 Malargüe, Argentina*

Full author list: https://www.auger.org/archive/authors_icrc_2025.html

^c*Deutsches Zentrum für Luft- und Raumfahrt (DLR German Aerospace Center), Institute of Atmospheric Physics, 82234 Oberpfaffenhofen, Germany*

E-mail: spokespersons@auger.org

The detection of side-scattered ultraviolet light from spaceborne lasers with fluorescence telescopes of cosmic ray observatories offers unique opportunities for systematic studies of the aerosol content of the local atmosphere. It also enables the validation of the optical calibration of the telescopes. Additionally, these observations provide valuable ground-based monitoring of the performance of the scientific instruments aboard satellites used for Earth climate observation.

Here, we report on results from the reconstruction of laser shots from the spaceborne lidar instrument ALADIN aboard the Aeolus satellite in 2019, 2020 and 2021. Furthermore, we present initial observations of laser shots from ATLID, the atmospheric lidar of the EarthCARE satellite, launched in 2024. EarthCARE's orbit is particularly well-suited for enabling laser detection within a few days at both the Pierre Auger Observatory and the Telescope Array Experiment, facilitating a relative calibration of the energy scales of these observatories.

39th International Cosmic Ray Conference (ICRC2025)
15–24 July 2025
Geneva, Switzerland



*Speaker

1. Introduction

Cosmic-ray observatories such as the Pierre Auger Observatory and the Telescope Array Experiment detect air showers with large-aperture ultraviolet (UV) fluorescence telescopes. To convert raw light tracks into accurate shower profiles, the state of the atmosphere needs to be known precisely, especially the density of aerosols that scatter and absorb the UV light. The standard tool to perform these measurements is to detect the side-scattered light from ground-based lasers [1–4] and ground-based lidar systems [5–7].

Space-based lasers have been observed previously by VERITAS [8] and TAIGA-HiSCORE [9, 10]. Recently, Earth-observation satellites have begun to carry high-energy UV lidars to profile winds, clouds, and aerosols on a global scale. The first mission equipped with an UV laser was Aeolus in 2018, followed up by EarthCARE in 2024. The lidar beams from these satellites are bright enough to be detected at astroparticle observatories that were built for detecting the far dimmer UV fluorescence and Cherenkov light from air showers. Here we report on the observations of UV laser tracks from Aeolus and EarthCARE with the Pierre Auger Observatory [11].

In these proceedings, we discuss how the detection of space-based lasers from the ground can be used to calibrate both space- and ground-based instruments. First, we summarize how the fluorescence telescopes of the Pierre Auger Observatory were used to ground-truth the lidar of the Aeolus satellite. We then present early results from the observation of laser shots from EarthCARE. The orbit of this satellite allows for a year-round observation, making it particularly useful to cross-check the standard aerosol reconstruction. Furthermore, the laser tracks of EarthCARE can be observed at the Pierre Auger Observatory in Argentina and the Telescope Array Experiment in USA within a few days during the same moon cycle. This opens the possibility for a direct cross-calibration of the energy scale of the two cosmic-ray observatories.

Together, these studies show that the collaboration between cosmic-ray observatories and space-based climate-sensing missions is mutually beneficial for understanding and calibrating both instruments.

2. Observation of Aeolus

The ESA Aeolus satellite (2018-2023) carried the UV Doppler wind lidar ALADIN. After the launch, the atmospheric back-scatter signal of the instrument declined and the identification of the root cause, losses on the emit or receive path, could not be unambiguously clarified. In mid-2019, the ultraviolet pulses were serendipitously recorded by the telescopes of fluorescence detector (FD) of the Pierre Auger Observatory. The 27 Schmidt-optics telescopes are optimised to detect the 300-400 nm fluorescence light from cosmic-ray air showers.

Since the FD is capable of detecting pulses of faint UV light, a measurement of the Aeolus laser using the telescopes of the Pierre Auger Observatory is possible, as illustrated in Fig. 1. Due to the nature of the sun-synchronous dusk-dawn orbit of Aeolus, it always passed close to the sunrise or sunset over any given point on the surface of the Earth. This limited the opportunities for measurements with the FD. Additionally to the aforementioned limitations by the moon-cycle, a measurement could only take place if the satellite passage time fell within the astronomical night, which occurred only during the southern-hemisphere winter months, i.e. between May and August.

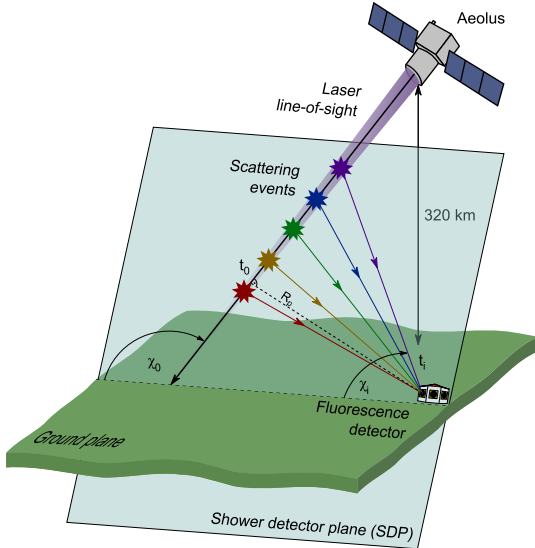


Figure 1: Geometry of the Aeolus laser beam being detected by one of the four fluorescence detectors of the Pierre Auger Observatory [12].

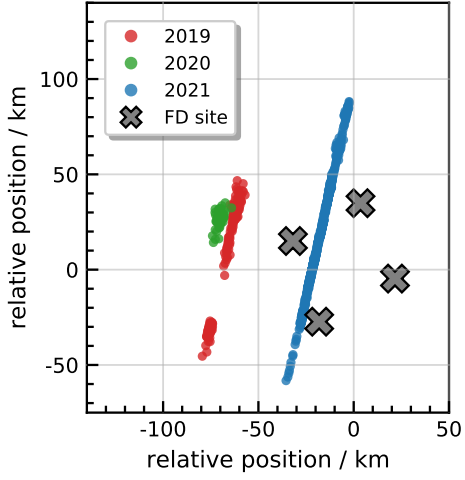


Figure 2: Measured laser impact point at an altitude of 1400 m for three sample Aeolus overpasses in the years 2019, 2020, and 2021 [12].

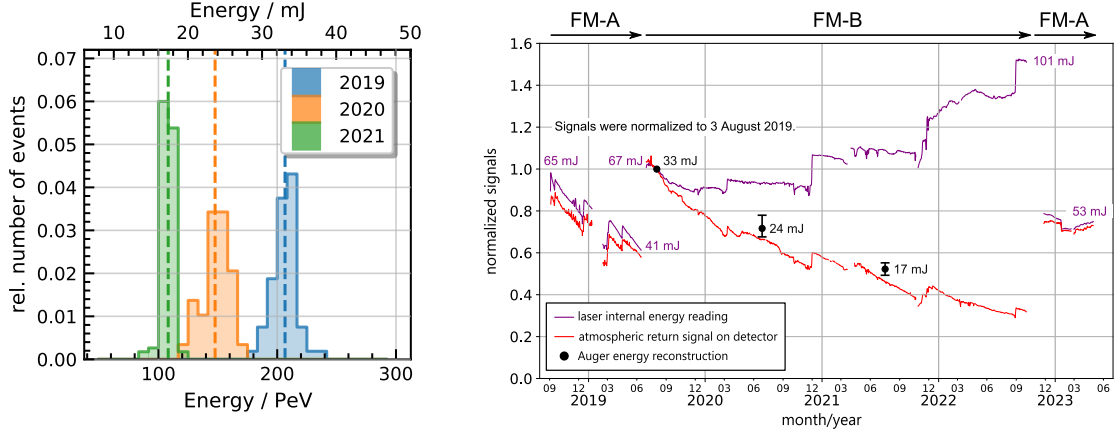
Furthermore, the orbit had a 7-day repeat cycle. Therefore, a measurement could only be performed once per week. Overall this resulted in up to six observations of the Aeolus laser per year, when clouds were not preventing the visibility.

These detections initiated a ground-based monitoring of the space laser and provided independent “ground truth” for both impact point (ground track) and pulse energy. In Ref. [12] we reported on three high-quality overpasses (3 Aug 2019, 27 Jun 2020, 17 Jul 2021) selected from 16 detections between 2019-2021, all taken in moonless, clear-sky winter nights when Aeolus crossed the array during astronomical darkness.

2.1 Geometrical reconstruction of the laser ground track

The Aeolus laser was visible in the FD due to the scattering of the laser beams with air molecules in the atmosphere. Similarly to the fluorescence light of showers, this light could be measured by the telescopes, creating an image of the laser beam in the camera constituting a line of pixels. This served as the basis for the geometrical reconstruction of the laser beam. If the beam was seen by only one telescope, the geometry could be obtained only by a so-called monocular reconstruction. Here we use an improved, zenith-angle-constrained, monocular reconstruction to determine the geometry of the laser track [13]. We first determined the average of the arrival direction of the laser beam from the combined data set, and then fix the direction during reconstruction to this average value, because the arrival direction of the laser beam does not change between the orbits. This reduces the number of geometry parameters from five to four, and it removes the usual near-degeneracies for the geometry within the shower-detector-plane (see 1).

The reconstructed impact points of the laser at an altitude of 1400 m (WGS84) for three sample overpasses in the years 2019, 2020, and 2021 is shown in Fig. 2. Notable is the change of the laser ground position for the year 2021 further to the East after an adjustment of the satellite orbit, which



(a) Reconstructed energies for three sample Aeolus overpasses in 2019, 2020, and 2021. The average energy per overpass is marked by the dashed line.

(b) Signal evolution of the Aeolus instrument: The purple curve represents the laser energy as measured at the output of the respective transmitter. The red curve denotes the atmospheric return signal that is detected on the Rayleigh receiver under clear-air conditions. The black dots indicate the Auger measurements, error bars denote statistical uncertainties.

Figure 3: Reconstruction of the Aeolus laser energy [12].

was obtained via a dedicated maneuver to allow for better measurements of the laser beam by the Observatory. The passages during the former two years happened at larger distances and thus fewer events and shorter tracks were observed.

When comparing the Aeolus ground track as determined by the Pierre Auger Observatory with the positions reported in the Aeolus data products, a horizontal offset of approximately 0.075° in longitude (6.8 km) became evident. This discrepancy was traced to an error in the Aeolus Level 1A (L1A) processor responsible for calculating the geolocation of Aeolus observations. In particular, the geolocation routines require time information along with a corresponding identifier specifying whether the time is in UTC (Coordinated Universal Time), GPS (Global Positioning System), or TAI (International Atomic Time). In two instances, an incorrect combination of time and identifier was passed to the geolocation routines, leading to slightly erroneous geolocation calculations.

The Auger observations of the Aeolus ground track also enabled an evaluation of the pointing accuracy and precision of the satellite. Auger data are available for each individual Aeolus laser pulse, whereas the Aeolus ground track in the L1A product is reported only at the measurement level, which corresponds to an average over 30 pulses. To enable a direct comparison, individual pulse times were reconstructed from the laser pulse frequency of 50.5 Hz and the measurement centroid times reported in the L1A product. The corresponding ground-track positions were then derived by time-based interpolation of the longitude and latitude values provided in the L1A data.

A pointing accuracy of 0.06 km along track and 0.82 km across track was determined. The result, expressed in 2σ , is 1.28 km along track and 0.93 km across track. These values represent a combination of Aeolus pointing errors, interpolation uncertainties, and Auger measurement errors, and therefore constitute upper limits on the true Aeolus pointing accuracy and precision. Nonetheless, they lie well within the Aeolus mission requirement of 2.0 km (2σ) for horizontal

geolocation, defined at the observation level averaged over 600 pulses.

2.2 Pulse-energy reconstruction

The fluorescence telescopes are absolutely calibrated with a 2.5 m diameter drum light source [14]. The uncertainty of the absolute calibration of the telescopes, including also contributions from the light-collection efficiency, reconstruction bias, molecular atmosphere, multiple scattering and the long-term calibration stability is 13 % [15, 16].

For every laser event the number of photo-electrons in the camera is converted to the received photon flux, corrected for atmospheric transmission (Rayleigh and aerosol optical depth) and distance from the telescope to the track. Taking furthermore into account the attenuation along the laser track, pulse energy at the spacecraft exit aperture is obtained. Simulations indicate a small ($\leq 3.7\%$) negative reconstruction bias, which is removed in the final numbers.

An energy reconstruction was performed for each individual laser track. Using the same three representative nights as for the geometry reconstruction, spanning the years 2019, 2020, and 2021, the resulting energy distributions are shown in Fig. 3a. For improved readability, the histograms were normalized to display relative rather than absolute event counts per bin. As can be seen, a steady decrease in reconstructed energy is observed over the years.

Figure 3b presents the temporal evolution of the ALADIN signal over the course of the Aeolus mission. The laser energy measured with a laser-internal photodiode is shown in purple, while the atmospheric return signal recorded by the onboard receiver is plotted in red. The latter is derived from the Rayleigh channel and restricted to observations under clear-air conditions to ensure predominantly molecular backscatter. Energy estimates obtained from the Auger laser-beam reconstruction are shown as black dots. To enable a direct comparison of signal evolution at different stages along the laser path (i.e., at the transmitter output, after atmospheric propagation as seen by Auger, and at the receiver) the signal levels are normalized to their respective values on 3 August 2019, the date of the first fiducial Auger measurement. In good approximation this normalization cancels out the systematic calibration uncertainty of the Auger energy estimates (13%), leaving only the statistical uncertainty. The uncertainty of the first measurement (normalized to unity) propagates into the relative uncertainties of the subsequent data points. The periods where different lasers were used, laser FM-A (Flight Model A) and FM-B, are indicated as arrows at the top of the plot.

The evolution of the energies reconstructed by the Auger Observatory closely follows the declining signal levels measured by ALADIN's receiver between 2019 and 2021. This agreement suggests that the observed signal loss during the FM-B laser operation originated along the emit path, i.e., between the laser output and the telescope. The Auger observations from July and August 2021 played a key role in supporting the root-cause analysis of this degradation and ultimately informed the decision to switch back to the FM-A laser in November 2022. Despite its lower output energy at the time of switchover (53 mJ instead of 101 mJ), the transition to FM-A resulted in a 2.2-fold increase in atmospheric return signal, bringing it back to the level seen during the initial FM-A period in early 2019. This full recovery of signal strength confirmed that the losses had occurred in the optical components unique to FM-B, most likely within the relay optics, which guide the FM-B beam onto the nominal optical axis. The specific loss mechanism remains under

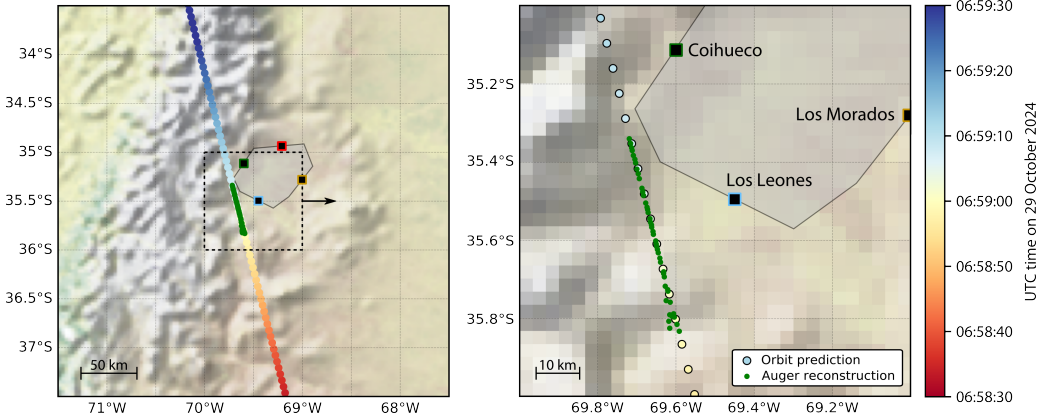


Figure 4: Reconstructed and predicted impact points of the EarthCARE laser at an altitude of 1400 m for the western pass near the Pierre Auger Observatory on 29 October 2024.

investigation. Current studies focus on laser-induced contamination, laser-induced damage, and bulk darkening of the optical elements as the most likely causes.

Interestingly, the energy reductions observed by the Auger Observatory in 2020 (-28%) and 2021 (-48%) relative to 2019 are slightly smaller than the corresponding losses measured at the ALADIN detectors (34% and -53%). This discrepancy suggests an additional degradation mechanism in the receive path, most likely a clipping of the atmospheric return signal at the field stop of the receiver.

It is also noteworthy that the absolute laser energy in 2019 reconstructed by the Auger Observatory (≈ 33 mJ) is lower than the value of 48 mJ expected at the telescope output. This indicates additional unaccounted losses in the emit path. An even larger discrepancy of about a factor of two compared to pre-launch simulations was already observed after launch in the atmospheric backscatter signals from the Rayleigh channel [17].

3. Observation of EarthCARE

The Atmospheric Lidar (ATLID) on ESA’s EarthCARE mission began routine UV (355 nm) operations in mid-2024. Within weeks, its ~ 35 mJ, 51 Hz pulses were detected by the fluorescence telescopes of the Pierre Auger Observatory and, shortly thereafter, by the fluorescence detector of the Telescope Array Experiment [18] and the Cherenkov telescopes of VERITAS [19].

Unlike Aeolus, whose dawn-dusk orbit limited visibility to a handful of winter nights, EarthCARE offers two nighttime passes over each site per 25-day repeat cycle – one “western” and one “eastern”. For Auger, the western and eastern overpasses together total 28 per year; roughly half of these fall into moonless measurement periods, so about 14 EarthCARE observations are feasible annually. Local overpass time is around 04:00, meaning that even at mid-summer the laser is visible before astronomical dawn. For the Telescope Array Experiment, the western pass is the closer of the two, occurring at about 03:00 local time, five days after the western Auger overpass and four days before the eastern one.

Using the same laser-reconstruction software developed for Aeolus, we reconstruct the ground track of the laser once again. Here we use an angle of 3° off nadir for the zenith-angle-constrained,

monocular reconstruction. As can be seen in Fig. 4, the reconstructed impact points for the overpass on the 29th of October 2024 are in good agreement with the ones expected from the EarthCARE orbit.

Beyond providing a well-timed global light source for fluorescence telescopes, EarthCARE data can improve and validate the standard Auger aerosol determination. By deriving vertical aerosol optical depth (VAOD) from EarthCARE laser tracks one can cross-check the VAOD profile reconstruction, since different distances between the laser shots and the telescopes can be sampled, as opposed to the standard analysis, in which the distance to the central laser facility is fixed (see Ref. [11] for a preliminary demonstration of this method). A second opportunity stems from the public ATLID aerosol products, which supply aerosol backscatter and extinction coefficients with 300 m horizontal resolution and vertical resolution of 100 m up to 20 km, and 500 m up to 40 km.

4. Summary and Outlook

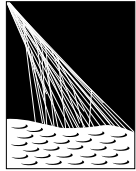
In these proceedings we reported the detection of spaceborne lasers with the Pierre Auger Observatory and presented a detailed analysis of lidar shots from the ALADIN instrument aboard Aeolus and reported on first observations of ATLID laser tracks from EarthCARE.

The successful ground-truthing of ATLID highlights the value of astroparticle observatories for validating and calibrating space-based lidar missions. Even more intriguing, from the perspective of ultra-high-energy cosmic-ray studies, is the reciprocal benefit: the lasers aboard EarthCARE and future missions provide an independent check on the aerosol profiles above each array. Acting as “standard candles,” they enable a global cross-calibration of cosmic-ray observatories and help reduce current uncertainties in the full-sky flux and anisotropy [20, 21]. This method of cross-calibrate a world-wide observatory can also be applied to the Cherenkov Telescope Array Observatory (CTAO) [22] and, using future spaceborne lidars, to the Global Cosmic Ray Observatory (GCOS) [23].

References

- [1] R. Abbasi *et al.*, [HiRes Coll.] *Astropart. Phys.* **25** (2006) 74.
- [2] B. Fick *et al.* *JINST* **1** no. 11, (2006) P11003.
- [3] P. Abreu *et al.*, [Pierre Auger Coll.] *JINST* **8** (2013) P04009.
- [4] Y. Takahashi *et al.*, [Telescope Array Coll.] *AIP Conf. Proc.* **1367** no. 1, (2011) 157.
- [5] T. Tomida *et al.* *Nucl. Instrum. Meth. A* **654** (2011) 653.
- [6] P. Abreu *et al.*, [Pierre Auger Coll.] *JINST* **7** (2012) P09001.
- [7] V. Rizi *et al.*, [Pierre Auger Coll.] *EPJ Web Conf.* **197** (2019) 02003.
- [8] G. M. Foote *et al.*, [VERITAS Coll.] *PoS ICRC2023* (2023) 1496.
- [9] A. Porelli *et al.* *PoS ICRC2017* (2018) 754.
- [10] A. Porelli, [TAIGA Coll.] *PoS ICRC2021* (2021) 876.
- [11] P. Abreu *et al.*, [Pierre Auger Coll.] *PoS ICRC2021* (2021) 235.
- [12] The Pierre Auger Collaboration, O. Lux, I. Krisch, O. Reitebuch, D. Huber, D. Wernham, and T. Parrinello *Optica* **11** no. 2, (2024) 263.
- [13] F. Knapp, “Analysis of Laser Shots of the Aeolus Satellite Observed with the Fluorescence Telescopes of the Pierre Auger Observatory,” Master’s thesis, Karlsruher Institut für Technologie, 2021.
- [14] J. T. Brack *et al.* *JINST* **8** (2013) P05014.
- [15] B. Dawson, [Pierre Auger Coll.] *PoS ICRC2019* (2020) 231.
- [16] V. Verzi, [Pierre Auger Coll.] *Proc. 33rd ICRC* (2013) 376.
- [17] O. Reitebuch *et al.* *EPJ Web Conf.* **237** (2020) 01010.
- [18] T. Fujii (OMU), private communication (2024).
- [19] G. Maier (DESY), private communication (2024).
- [20] L. Caccianiga *et al.*, [Pierre Auger and Telescope Array Coll.] *PoS ICRC2023* (2023) 521.
- [21] T. Tsunesada *et al.*, [Pierre Auger and Telescope Array Coll.] *PoS ICRC2023* (2023) 406.
- [22] M. Actis *et al.*, [CTA Coll.] *Exper. Astron.* **32** (2011) 1936.
- [23] M. Ahlers *et al.* [arXiv:2502.05657](https://arxiv.org/abs/2502.05657).

The Pierre Auger Collaboration



**PIERRE
AUGER
OBSERVATORY**

- A. Abdul Halim¹³, P. Abreu⁷⁰, M. Aglietta^{53,51}, I. Allekotte¹, K. Almeida Cheminant^{78,77}, A. Almela^{7,12}, R. Aloisio^{44,45}, J. Alvarez-Muñiz⁷⁶, A. Ambrosone⁴⁴, J. Ammerman Yebra⁷⁶, G.A. Anastasi^{57,46}, L. Anchordoqui⁸³, B. Andrade⁷, L. Andrade Dourado^{44,45}, S. Andringa⁷⁰, L. Apollonio^{58,48}, C. Aramo⁴⁹, E. Arnone^{62,51}, J.C. Arteaga Velázquez⁶⁶, P. Assis⁷⁰, G. Avila¹¹, E. Avocone^{56,45}, A. Bakalova³¹, F. Barbato^{44,45}, A. Bartz Mocellin⁸², J.A. Bellido¹³, C. Berat³⁵, M.E. Bertaina^{62,51}, M. Bianciotto^{62,51}, P.L. Biermann^a, V. Binet⁵, K. Bismarck^{38,7}, T. Bister^{77,78}, J. Biteau^{36,i}, J. Blazek³¹, J. Blümer⁴⁰, M. Boháčová³¹, D. Boncioli^{56,45}, C. Bonifazi⁸, L. Bonneau Arbeletche²², N. Borodai⁶⁸, J. Brack^f, P.G. Brichetto Orchera^{7,40}, F.L. Briechle⁴¹, A. Bueno⁷⁵, S. Buitink¹⁵, M. Buscemi^{46,57}, M. Büskens^{38,7}, A. Bwembya^{77,78}, K.S. Caballero-Mora⁶⁵, S. Cabana-Freire⁷⁶, L. Caccianiga^{58,48}, F. Campuzano⁶, J. Caraça-Valente⁸², R. Caruso^{57,46}, A. Castellina^{53,51}, F. Catalani¹⁹, G. Cataldi⁴⁷, L. Cazon⁷⁶, M. Cerda¹⁰, B. Čermáková⁴⁰, A. Cermenati^{44,45}, J.A. Chinellato²², J. Chudoba³¹, L. Chytko³², R.W. Clay¹³, A.C. Cobos Cerutti⁶, R. Colalillo^{59,49}, R. Conceição⁷⁰, G. Consolati^{48,54}, M. Conte^{55,47}, F. Convenga^{44,45}, D. Correia dos Santos²⁷, P.J. Costa⁷⁰, C.E. Covault⁸¹, M. Cristinziani⁴³, C.S. Cruz Sanchez³, S. Dasso^{4,2}, K. Daumiller⁴⁰, B.R. Dawson¹³, R.M. de Almeida²⁷, E.-T. de Boone⁴³, B. de Errico²⁷, J. de Jesús⁷, S.J. de Jong^{77,78}, J.R.T. de Mello Neto²⁷, I. De Mitri^{44,45}, J. de Oliveira¹⁸, D. de Oliveira Franco⁴², F. de Palma^{55,47}, V. de Souza²⁰, E. De Vito^{55,47}, A. Del Popolo^{57,46}, O. Deligny³³, N. Denner³¹, L. Deval^{53,51}, A. di Matteo⁵¹, C. Dobrigkeit²², J.C. D'Olivo⁶⁷, L.M. Domingues Mendes^{16,70}, Q. Dorost⁴³, J.C. dos Anjos¹⁶, R.C. dos Anjos²⁶, J. Ebr³¹, F. Ellwanger⁴⁰, R. Engel^{38,40}, I. Epicoco^{55,47}, M. Erdmann⁴¹, A. Etchegoyen^{7,12}, C. Evoli^{44,45}, H. Falcke^{77,79,78}, G. Farrar⁸⁵, A.C. Fauth²², T. Fehler⁴³, F. Feldbusch³⁹, A. Fernandes⁷⁰, M. Fernandez¹⁴, B. Fick⁸⁴, J.M. Figueira⁷, P. Filip^{38,7}, A. Filipčić^{74,73}, T. Fitoussi⁴⁰, B. Flagg⁸⁷, T. Fodran⁷⁷, A. Franco⁴⁷, M. Freitas⁷⁰, T. Fujii^{86,h}, A. Fuster^{7,12}, C. Galea⁷⁷, B. García⁶, C. Gaudí³⁷, P.L. Ghia³³, U. Giaccari⁴⁷, F. Gobbi¹⁰, F. Gollan⁷, G. Golup¹, M. Gómez Berisso¹, P.F. Gómez Vitale¹¹, J.P. Gongora¹¹, J.M. González¹, N. González⁷, D. Góra⁶⁸, A. Gorgi^{53,51}, M. Gottowik⁴⁰, F. Guarino^{59,49}, G.P. Guedes²³, L. Gültzow⁴⁰, S. Hahn³⁸, P. Hamal³¹, M.R. Hampel⁷, P. Hansen³, V.M. Harvey¹³, A. Haungs⁴⁰, T. Hebbeker⁴¹, C. Hojvat^d, J.R. Hörandel^{77,78}, P. Horvath³², M. Hrabovský³², T. Huege^{40,15}, A. Insolia^{57,46}, P.G. Isar⁷², M. Ismaiel^{77,78}, P. Janecek³¹, V. Jilek³¹, K.-H. Kampert³⁷, B. Keilhauer⁴⁰, A. Khakurdikar⁷⁷, V.V. Kizakke Covilakam^{7,40}, H.O. Klages⁴⁰, M. Kleifges³⁹, J. Köhler⁴⁰, F. Krieger⁴¹, M. Kubatova³¹, N. Kunka³⁹, B.L. Lago¹⁷, N. Langner⁴¹, N. Leal⁷, M.A. Leigui de Oliveira²⁵, Y. Lema-Capeans⁷⁶, A. Letessier-Selvon³⁴, I. Lhenry-Yvon³³, L. Lopes⁷⁰, J.P. Lundquist⁷³, M. Mallamaci^{60,46}, D. Mandat³¹, P. Mantelsch^d, F.M. Mariani^{58,48}, A.G. Mariazzi³, I.C. Marić¹⁴, G. Marsella^{60,46}, D. Martello^{55,47}, S. Martinelli^{40,7}, M.A. Martins⁷⁶, H.-J. Mathes⁴⁰, J. Matthews⁸, G. Matthiae^{61,50}, E. Mayotte⁸², S. Mayotte⁸², P.O. Mazur^d, G. Medina-Tanco⁶⁷, J. Meinert³⁷, D. Melo⁷, A. Menshikov³⁹, C. Merx⁴⁰, S. Michal³¹, M.I. Micheletti⁵, L. Miramonti^{58,48}, M. Mogarkar⁶⁸, S. Mollerach¹, F. Montanet³⁵, L. Morejon³⁷, K. Mulrey^{77,78}, R. Mussa⁵¹, W.M. Namasaka³⁷, S. Negi³¹, L. Nellen⁶⁷, K. Nguyen⁸⁴, G. Nicora⁹, M. Niechciol⁴³, D. Nitz⁸⁴, D. Nosek³⁰, A. Novikov⁸⁷, V. Novotny³⁰, L. Nožka³², A. Nucita^{55,47}, L.A. Núñez²⁹, J. Ochoa^{7,40}, C. Oliveira²⁰, L. Östman³¹, M. Palatka³¹, J. Pallotta⁹, S. Panja³¹, G. Parente⁷⁶, T. Paulsen³⁷, J. Pawlowsky³⁷, M. Pech³¹, J. Pěkala⁶⁸, R. Pelayo⁶⁴, V. Pelgrims¹⁴, L.A.S. Pereira²⁴, E.E. Pereira Martins^{38,7}, C. Pérez Bertolli^{7,40}, L. Perrone^{55,47}, S. Petrera^{44,45}, C. Petrucci⁵⁶, T. Pierog⁴⁰, M. Pimenta⁷⁰, M. Platino⁷, B. Pont⁷⁷, M. Pourmohammad Shahvar^{60,46}, P. Privitera⁸⁶, C. Priyadarshi⁶⁸, M. Prouza³¹, K. Pytel⁶⁹, S. Querchfeld³⁷, J. Rautenberg³⁷, D. Ravignani⁷, J.V. Reginatto Akim²², A. Reuzki⁴¹, J. Ridky³¹, F. Riehn^{76,j}, M. Risse⁴³, V. Rizi^{56,45}, E. Rodriguez^{7,40}, G. Rodriguez Fernandez⁵⁰, J. Rodriguez Rojo¹¹, S. Rossoni⁴², M. Roth⁴⁰, E. Roulet¹, A.C. Rovero⁴, A. Saftoiu⁷¹, M. Saharan⁷⁷, F. Salamida^{56,45}, H. Salazar⁶³, G. Salina⁵⁰, P. Sampathkumar⁴⁰, N. San Martin⁸², J.D. Sanabria Gomez²⁹, F. Sánchez⁷, E.M. Santos²¹, E. Santos³¹, F. Sarazin⁸², R. Sarmento⁷⁰, R. Sato¹¹, P. Savina^{44,45}, V. Scherini^{55,47}, H. Schieler⁴⁰, M. Schimassek³³, M. Schimp³⁷, D. Schmidt⁴⁰, O. Scholten^{15,b}, H. Schoorlemmer^{77,78}, P. Schovánek³¹, F.G. Schröder^{87,40}, J. Schulte⁴¹, T. Schulz³¹, S.J. Scιutto³, M. Scornavacche⁷, A. Sedoski⁷, A. Segreto^{52,46}, S. Sehgal³⁷, S.U. Shivashankara⁷³, G. Sig⁴², K. Simkova^{15,14}, F. Simon³⁹, R. Šmíd⁸⁶, P. Sommers^e, R. Squartini¹⁰, M. Stadelmaier^{40,48,58}, S. Stanic⁷³, J. Stasielak⁶⁸, P. Stassi³⁵, S. Strähnz³⁸, M. Straub⁴¹, T. Suomijärvi³⁶, A.D. Supanitsky⁷, Z. Svozilikova³¹, K. Syrokvas³⁰, Z. Szadkowski⁶⁹, F. Tairli¹³, M. Tambone^{59,49}, A. Tapia²⁸, C. Taricco^{62,51}, C. Timmermans^{78,77}, O. Tkachenko³¹, P. Tobiska³¹, C.J. Todero Peixoto¹⁹, B. Tome⁷⁰, A. Travaini¹⁰, P. Travnicek³¹, M. Tueros³, M. Unger⁴⁰, R. Uzeiroska³⁷, L. Vaclavek³², M. Vacula³², I. Vaiman^{44,45}, J.F. Valdés Galicia⁶⁷, L. Valore^{59,49}, P. van Dillen^{77,78}, E. Varela⁶³, V. Vašíčková³⁷, A. Vásquez-Ramírez²⁹, D. Veberič⁴⁰, I.D. Vergara Quispe³, S. Verpoest⁸⁷, V. Verzli⁵⁰, J. Vicha³¹, J. Vink⁸⁰, S. Vorobiov⁷³, J.B. Vuta³¹, C. Watanabe²⁷, A.A. Watson^c, A. Weindl⁴⁰, M. Weitz³⁷, L. Wiencke⁸², H. Wilczyński⁶⁸, B. Wundheiler⁷, B. Yue³⁷, A. Yushkov³¹, E. Zas⁷⁶, D. Zavrtanik^{73,74}, M. Zavrtanik^{74,73}

- ¹ Centro Atómico Bariloche and Instituto Balseiro (CNEA-UNCuyo-CONICET), San Carlos de Bariloche, Argentina
- ² Departamento de Física and Departamento de Ciencias de la Atmósfera y los Océanos, FCEyN, Universidad de Buenos Aires and CONICET, Buenos Aires, Argentina
- ³ IFLP, Universidad Nacional de La Plata and CONICET, La Plata, Argentina
- ⁴ Instituto de Astronomía y Física del Espacio (IAFE, CONICET-UBA), Buenos Aires, Argentina
- ⁵ Instituto de Física de Rosario (IFIR) – CONICET/U.N.R. and Facultad de Ciencias Bioquímicas y Farmacéuticas U.N.R., Rosario, Argentina
- ⁶ Instituto de Tecnologías en Detección y Astropartículas (CNEA, CONICET, UNSAM), and Universidad Tecnológica Nacional – Facultad Regional Mendoza (CONICET/CNEA), Mendoza, Argentina
- ⁷ Instituto de Tecnologías en Detección y Astropartículas (CNEA, CONICET, UNSAM), Buenos Aires, Argentina
- ⁸ International Center of Advanced Studies and Instituto de Ciencias Físicas, ECyT-UNSAM and CONICET, Campus Miguelete – San Martín, Buenos Aires, Argentina
- ⁹ Laboratorio Atmósfera – Departamento de Investigaciones en Láseres y sus Aplicaciones – UNIDEF (CITEDEF-CONICET), Argentina
- ¹⁰ Observatorio Pierre Auger, Malargüe, Argentina
- ¹¹ Observatorio Pierre Auger and Comisión Nacional de Energía Atómica, Malargüe, Argentina
- ¹² Universidad Tecnológica Nacional – Facultad Regional Buenos Aires, Buenos Aires, Argentina
- ¹³ University of Adelaide, Adelaide, S.A., Australia
- ¹⁴ Université Libre de Bruxelles (ULB), Brussels, Belgium
- ¹⁵ Vrije Universiteit Brussels, Brussels, Belgium
- ¹⁶ Centro Brasileiro de Pesquisas Fisicas, Rio de Janeiro, RJ, Brazil
- ¹⁷ Centro Federal de Educação Tecnológica Celso Suckow da Fonseca, Petropolis, Brazil
- ¹⁸ Instituto Federal de Educação, Ciência e Tecnologia do Rio de Janeiro (IFRJ), Brazil
- ¹⁹ Universidade de São Paulo, Escola de Engenharia de Lorena, Lorena, SP, Brazil
- ²⁰ Universidade de São Paulo, Instituto de Física de São Carlos, São Carlos, SP, Brazil
- ²¹ Universidade de São Paulo, Instituto de Física, São Paulo, SP, Brazil
- ²² Universidade Estadual de Campinas (UNICAMP), IFGW, Campinas, SP, Brazil
- ²³ Universidade Estadual de Feira de Santana, Feira de Santana, Brazil
- ²⁴ Universidade Federal de Campina Grande, Centro de Ciencias e Tecnologia, Campina Grande, Brazil
- ²⁵ Universidade Federal do ABC, Santo André, SP, Brazil
- ²⁶ Universidade Federal do Paraná, Setor Palotina, Palotina, Brazil
- ²⁷ Universidade Federal do Rio de Janeiro, Instituto de Física, Rio de Janeiro, RJ, Brazil
- ²⁸ Universidad de Medellín, Medellín, Colombia
- ²⁹ Universidad Industrial de Santander, Bucaramanga, Colombia
- ³⁰ Charles University, Faculty of Mathematics and Physics, Institute of Particle and Nuclear Physics, Prague, Czech Republic
- ³¹ Institute of Physics of the Czech Academy of Sciences, Prague, Czech Republic
- ³² Palacky University, Olomouc, Czech Republic
- ³³ CNRS/IN2P3, IJCLab, Université Paris-Saclay, Orsay, France
- ³⁴ Laboratoire de Physique Nucléaire et de Hautes Energies (LPNHE), Sorbonne Université, Université de Paris, CNRS-IN2P3, Paris, France
- ³⁵ Univ. Grenoble Alpes, CNRS, Grenoble Institute of Engineering Univ. Grenoble Alpes, LPSC-IN2P3, 38000 Grenoble, France
- ³⁶ Université Paris-Saclay, CNRS/IN2P3, IJCLab, Orsay, France
- ³⁷ Bergische Universität Wuppertal, Department of Physics, Wuppertal, Germany
- ³⁸ Karlsruhe Institute of Technology (KIT), Institute for Experimental Particle Physics, Karlsruhe, Germany
- ³⁹ Karlsruhe Institute of Technology (KIT), Institut für Prozessdatenverarbeitung und Elektronik, Karlsruhe, Germany
- ⁴⁰ Karlsruhe Institute of Technology (KIT), Institute for Astroparticle Physics, Karlsruhe, Germany
- ⁴¹ RWTH Aachen University, III. Physikalisches Institut A, Aachen, Germany
- ⁴² Universität Hamburg, II. Institut für Theoretische Physik, Hamburg, Germany
- ⁴³ Universität Siegen, Department Physik – Experimentelle Teilchenphysik, Siegen, Germany
- ⁴⁴ Gran Sasso Science Institute, L'Aquila, Italy
- ⁴⁵ INFN Laboratori Nazionali del Gran Sasso, Assergi (L'Aquila), Italy
- ⁴⁶ INFN, Sezione di Catania, Catania, Italy
- ⁴⁷ INFN, Sezione di Lecce, Lecce, Italy
- ⁴⁸ INFN, Sezione di Milano, Milano, Italy
- ⁴⁹ INFN, Sezione di Napoli, Napoli, Italy
- ⁵⁰ INFN, Sezione di Roma "Tor Vergata", Roma, Italy
- ⁵¹ INFN, Sezione di Torino, Torino, Italy

- ⁵² Istituto di Astrofisica Spaziale e Fisica Cosmica di Palermo (INAF), Palermo, Italy
⁵³ Osservatorio Astrofisico di Torino (INAF), Torino, Italy
⁵⁴ Politecnico di Milano, Dipartimento di Scienze e Tecnologie Aerospaziali , Milano, Italy
⁵⁵ Università del Salento, Dipartimento di Matematica e Fisica “E. De Giorgi”, Lecce, Italy
⁵⁶ Università dell’Aquila, Dipartimento di Scienze Fisiche e Chimiche, L’Aquila, Italy
⁵⁷ Università di Catania, Dipartimento di Fisica e Astronomia “Ettore Majorana“, Catania, Italy
⁵⁸ Università di Milano, Dipartimento di Fisica, Milano, Italy
⁵⁹ Università di Napoli “Federico II”, Dipartimento di Fisica “Ettore Pancini”, Napoli, Italy
⁶⁰ Università di Palermo, Dipartimento di Fisica e Chimica ”E. Segrè”, Palermo, Italy
⁶¹ Università di Roma “Tor Vergata”, Dipartimento di Fisica, Roma, Italy
⁶² Università Torino, Dipartimento di Fisica, Torino, Italy
⁶³ Benemérita Universidad Autónoma de Puebla, Puebla, México
⁶⁴ Unidad Profesional Interdisciplinaria en Ingeniería y Tecnologías Avanzadas del Instituto Politécnico Nacional (UPIITA-IPN), México, D.F., México
⁶⁵ Universidad Autónoma de Chiapas, Tuxtla Gutiérrez, Chiapas, México
⁶⁶ Universidad Michoacana de San Nicolás de Hidalgo, Morelia, Michoacán, México
⁶⁷ Universidad Nacional Autónoma de México, México, D.F., México
⁶⁸ Institute of Nuclear Physics PAN, Krakow, Poland
⁶⁹ University of Łódź, Faculty of High-Energy Astrophysics, Łódź, Poland
⁷⁰ Laboratório de Instrumentação e Física Experimental de Partículas – LIP and Instituto Superior Técnico – IST, Universidade de Lisboa – UL, Lisboa, Portugal
⁷¹ “Horia Hulubei” National Institute for Physics and Nuclear Engineering, Bucharest-Magurele, Romania
⁷² Institute of Space Science, Bucharest-Magurele, Romania
⁷³ Center for Astrophysics and Cosmology (CAC), University of Nova Gorica, Nova Gorica, Slovenia
⁷⁴ Experimental Particle Physics Department, J. Stefan Institute, Ljubljana, Slovenia
⁷⁵ Universidad de Granada and C.A.F.P.E., Granada, Spain
⁷⁶ Instituto Galego de Física de Altas Enerxías (IGFAE), Universidade de Santiago de Compostela, Santiago de Compostela, Spain
⁷⁷ IMAPP, Radboud University Nijmegen, Nijmegen, The Netherlands
⁷⁸ Nationaal Instituut voor Kernfysica en Hoge Energie Fysica (NIKHEF), Science Park, Amsterdam, The Netherlands
⁷⁹ Stichting Astronomisch Onderzoek in Nederland (ASTRON), Dwingeloo, The Netherlands
⁸⁰ Universiteit van Amsterdam, Faculty of Science, Amsterdam, The Netherlands
⁸¹ Case Western Reserve University, Cleveland, OH, USA
⁸² Colorado School of Mines, Golden, CO, USA
⁸³ Department of Physics and Astronomy, Lehman College, City University of New York, Bronx, NY, USA
⁸⁴ Michigan Technological University, Houghton, MI, USA
⁸⁵ New York University, New York, NY, USA
⁸⁶ University of Chicago, Enrico Fermi Institute, Chicago, IL, USA
⁸⁷ University of Delaware, Department of Physics and Astronomy, Bartol Research Institute, Newark, DE, USA

^a Max-Planck-Institut für Radioastronomie, Bonn, Germany^b also at Kapteyn Institute, University of Groningen, Groningen, The Netherlands^c School of Physics and Astronomy, University of Leeds, Leeds, United Kingdom^d Fermi National Accelerator Laboratory, Fermilab, Batavia, IL, USA^e Pennsylvania State University, University Park, PA, USA^f Colorado State University, Fort Collins, CO, USA^g Louisiana State University, Baton Rouge, LA, USA^h now at Graduate School of Science, Osaka Metropolitan University, Osaka, Japanⁱ Institut universitaire de France (IUF), France^j now at Technische Universität Dortmund and Ruhr-Universität Bochum, Dortmund and Bochum, Germany

Acknowledgments

The successful installation, commissioning, and operation of the Pierre Auger Observatory would not have been possible without the strong commitment and effort from the technical and administrative staff in Malargüe. We are very grateful to the following agencies and organizations for financial support:

Argentina – Comisión Nacional de Energía Atómica; Agencia Nacional de Promoción Científica y Tecnológica (ANPCyT); Consejo Nacional de Investigaciones Científicas y Técnicas (CONICET); Gobierno de la Provincia de

Mendoza; Municipalidad de Malargüe; NDM Holdings and Valle Las Leñas; in gratitude for their continuing cooperation over land access; Australia – the Australian Research Council; Belgium – Fonds de la Recherche Scientifique (FNRS); Research Foundation Flanders (FWO), Marie Curie Action of the European Union Grant No. 101107047; Brazil – Conselho Nacional de Desenvolvimento Científico e Tecnológico (CNPq); Financiadora de Estudos e Projetos (FINEP); Fundação de Amparo à Pesquisa do Estado de Rio de Janeiro (FAPERJ); São Paulo Research Foundation (FAPESP) Grants No. 2019/10151-2, No. 2010/07359-6 and No. 1999/05404-3; Ministério da Ciência, Tecnologia, Inovações e Comunicações (MCTIC); Czech Republic – GACR 24-13049S, CAS LQ100102401, MEYS LM2023032, CZ.02.1.01/0.0/0.0/16_013/0001402, CZ.02.1.01/0.0/0.0/18_046/0016010 and CZ.02.1.01/0.0/0.0/17_049/0008422 and CZ.02.01.01/00/22_008/0004632; France – Centre de Calcul IN2P3/CNRS; Centre National de la Recherche Scientifique (CNRS); Conseil Régional Ile-de-France; Département Physique Nucléaire et Corpusculaire (PNC-IN2P3/CNRS); Département Sciences de l'Univers (SDU-INSU/CNRS); Institut Lagrange de Paris (ILP) Grant No. LABEX ANR-10-LABX-63 within the Investissements d'Avenir Programme Grant No. ANR-11-IDEX-0004-02; Germany – Bundesministerium für Bildung und Forschung (BMBF); Deutsche Forschungsgemeinschaft (DFG); Finanzministerium Baden-Württemberg; Helmholtz Alliance for Astroparticle Physics (HAP); Helmholtz-Gemeinschaft Deutscher Forschungszentren (HGF); Ministerium für Kultur und Wissenschaft des Landes Nordrhein-Westfalen; Ministerium für Wissenschaft, Forschung und Kunst des Landes Baden-Württemberg; Italy – Istituto Nazionale di Fisica Nucleare (INFN); Istituto Nazionale di Astrofisica (INAF); Ministero dell'Università e della Ricerca (MUR); CETEMPS Center of Excellence; Ministero degli Affari Esteri (MAE), ICSC Centro Nazionale di Ricerca in High Performance Computing, Big Data and Quantum Computing, funded by European Union NextGenerationEU, reference code CN_00000013; México – Consejo Nacional de Ciencia y Tecnología (CONACYT) No. 167733; Universidad Nacional Autónoma de México (UNAM); PAPIIT DGAPA-UNAM; The Netherlands – Ministry of Education, Culture and Science; Netherlands Organisation for Scientific Research (NWO); Dutch national e-infrastructure with the support of SURF Cooperative; Poland – Ministry of Education and Science, grants No. DIR/WK/2018/11 and 2022/WK/12; National Science Centre, grants No. 2016/22/M/ST9/00198, 2016/23/B/ST9/01635, 2020/39/B/ST9/01398, and 2022/45/B/ST9/02163; Portugal – Portuguese national funds and FEDER funds within Programa Operacional Factores de Competitividade through Fundação para a Ciência e a Tecnologia (COMPETE); Romania – Ministry of Research, Innovation and Digitization, CNCS-UEFISCDI, contract no. 30N/2023 under Romanian National Core Program LAPLAS VII, grant no. PN 23 21 01 02 and project number PN-III-P1-1.1-TE-2021-0924/TE57/2022, within PNCDI III; Slovenia – Slovenian Research Agency, grants P1-0031, P1-0385, I0-0033, N1-0111; Spain – Ministerio de Ciencia e Innovación/Agencia Estatal de Investigación (PID2019-105544GB-I00, PID2022-140510NB-I00 and RYC2019-027017-I), Xunta de Galicia (CIGUS Network of Research Centers, Consolidación 2021 GRC GI-2033, ED431C-2021/22 and ED431F-2022/15), Junta de Andalucía (SOMM17/6104/UGR and P18-FR-4314), and the European Union (Marie Skłodowska-Curie 101065027 and ERDF); USA – Department of Energy, Contracts No. DE-AC02-07CH11359, No. DE-FR02-04ER41300, No. DE-FG02-99ER41107 and No. DE-SC0011689; National Science Foundation, Grant No. 0450696, and NSF-2013199; The Grainger Foundation; Marie Curie-IRSES/EPLANET; European Particle Physics Latin American Network; and UNESCO.